

Fluorescence quantum yield of carbon dioxide for quantitative UV laser-induced fluorescence in high-pressure flames

T. Lee · W.G. Bessler · J. Yoo · C. Schulz · J.B. Jeffries · R.K. Hanson

Received: 3 March 2008 / Revised version: 14 July 2008 / Published online: 4 September 2008
© Springer-Verlag 2008

Abstract The fluorescence quantum yield for ultraviolet laser-induced fluorescence of CO₂ is determined for selected excitation wavelengths in the range 215–250 nm. Wavelength-resolved laser-induced fluorescence (LIF) spectra of CO₂, NO, and O₂ are measured in the burned gases of a laminar CH₄/air flame ($\phi = 0.9$ and 1.1) at 20 bar with additional NO seeded into the flow. The fluorescence spectra are fit to determine the relative contribution of the three species to infer an estimate of fluorescence quantum yield for CO₂ that ranges from $2\text{--}8 \times 10^{-6}$ depending on temperature and excitation wavelength with an estimated uncertainty of $\pm 0.5 \times 10^{-6}$. The CO₂ fluorescence signal increases linearly with gas pressure for flames with constant CO₂ mole fraction for the 10 to 60 bar range, indicating that collisional quenching is not an important contributor to the CO₂ fluorescence quantum yield. Spectral simulation calculations are used to choose two wavelengths for excitation of CO₂, 239.34 and 242.14 nm, which minimize interference from

LIF of NO and O₂. Quantitative LIF images of CO₂ are demonstrated using these two excitation wavelengths and the measured fluorescence quantum yield.

PACS 42.62.Fi · 42.30.Va · 47.70.Pq · 07.35.+k · 39.30.+w

1 Introduction

This paper investigates the use of laser-induced fluorescence (LIF) to image hot CO₂ in the burned gases of high-pressure flames using excitation with pulsed lasers in the ultraviolet (UV). These new results build on earlier work that identified UV LIF from hot CO₂ in high-pressure combustion products [1], and on qualitative planar LIF (PLIF) measurements [2] in flames at 20 bar that illustrated the feasibility for imaging the spatial distribution of hot CO₂.

LIF can be species- and quantum-state selective, enabling measurements of key combustion parameters (i.e., species concentration, temperature, pressure, density, and velocity, as well as provide a monitor to follow reaction chemistry) and is widely used for combustion research [3–5]. Although LIF imaging strategies exist for several important chemical intermediates and combustion byproducts such as NO, OH, CH, O₂, etc., published strategies for LIF detection of CO₂ are mostly limited to infrared excitation and detection using vibrational transitions [6, 7]. Unfortunately, IR LIF using vibrational transitions involves complex energy transfer, weak signals, and the need for advanced infrared-camera technology. In this respect, an ultraviolet method for quantitative CO₂ imaging is a desirable alternative. The results and discussion in this study demonstrate the ability for quantitative UV CO₂-LIF measurements in high-pressure, high-temperature systems, and the CO₂ fluorescence quantum

T. Lee (✉) · J. Yoo · J.B. Jeffries · R.K. Hanson
High Temperature Gasdynamics Laboratory, Department
of Mechanical Engineering, Stanford University, Stanford,
CA 94305, USA
e-mail: tonghun@msu.edu
Fax: +1-517-3531750

Present address:

T. Lee
Department of Mechanical Engineering, Michigan State
University, East Lansing, MI 48824, USA

W.G. Bessler
Institute of Technical Thermodynamics, German Aerospace
Center, Pfaffenwaldring 38–40, 70569 Stuttgart, Germany

C. Schulz
IVG, University of Duisburg-Essen, Lotharstrasse 1,
47057 Duisburg, Germany

yield measurements also provide an insight into the photo-physics of UV excitation and fluorescence of CO₂.

The work presented here extends our earlier imaging measurements of CO₂ combustion products in fuel-lean CH₄/air flames to $10 \leq p \leq 60$ bar. A brief discussion of the spectroscopy of energy levels involved in the electronic excitation and laser-induced fluorescence of CO₂ is also presented. For the first time we investigate the CO₂ fluorescence quantum yield (Φ_{FQY}) and find that it is pressure independent for this range. A series of wavelength-resolved LIF measurements in the burned gases of a lean flame at 20 bar are combined with our early work that measured the CO₂ absorption cross-section [3] and these data are used to determine the temperature (1760–2025 K) and wavelength (215–250 nm) dependence of Φ_{FQY} of CO₂ relative to that of NO. Using the known NO concentration, absorption cross-section and fluorescence quantum yield as a calibration, quantitative LIF images of CO₂ in the burned gases of CH₄/air flames are presented for $10 \leq p \leq 60$ bar; Φ_{FQY} is found to be independent of pressure over this range.

2 Background

2.1 Previous work on UV CO₂ LIF

Two observations during our studies of nitric oxide (NO) LIF in high-pressure flames [8–10] motivated our earlier investigation of CO₂ LIF [1, 2]. First, the severe attenuation of the UV probe laser and LIF signal in high-pressure flames suggested strong optical absorption in high-temperature, high-pressure combustion products. The UV laser light attenuation in some cases reached as much as 40% over a distance of only about 1 cm (at the excitation wavelength of 226 nm at 60 bar). Subsequently, the main absorbing species responsible for this attenuation was identified as hot, vibrationally excited carbon dioxide (CO₂) [11], and the UV absorption cross-sections between 190 and 320 nm CO₂ were measured for $880 < T < 3050$ K in shock-heated gas mixtures [12–14]. Second, pervasive broadband emission was observed that overlaps with the γ bands of NO and the Schumann–Runge bands of O₂ (200–450 nm). Our previous studies of CH₄/air and CH₄/Ar/O₂ high-pressure flames identified this interference as CO₂ LIF [1]. Typical emission from NO LIF in a fuel lean 40 bar CH₄/air flame is shown in Fig. 1. The contributions from LIF of NO and O₂ are identified by using spectral simulations and combined using a non-linear multi-parameter fitting routine. As can be seen in the lower panel in Fig. 1 the significant broadband contribution from CO₂ LIF is present throughout the spectrum.

For planar laser-induced fluorescence (PLIF) of CO₂, excitation wavelengths were chosen to minimize the excitation

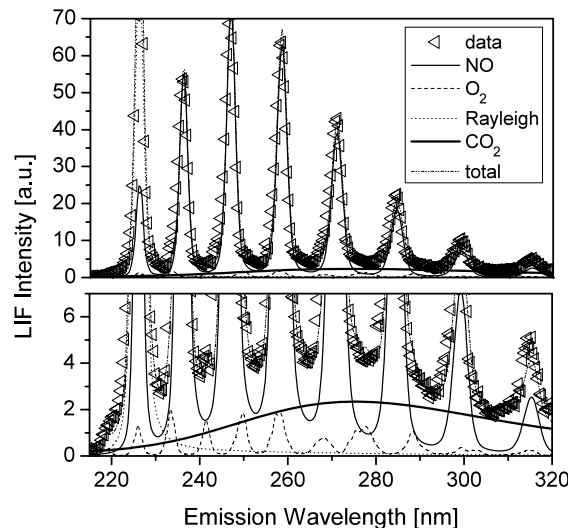


Fig. 1 Emission from laser excitation at 226.03 nm (lean 40 bar CH₄/air flame). CO₂ LIF is the broadband emission across the entire region

of NO and O₂ to discriminate CO₂ LIF against contributions from these species. In our previous study, qualitative CO₂ LIF images were acquired in a 20 bar CH₄/air flame [2] using this strategy. The present study extends CO₂ UV PLIF to flames from 10 to 60 bar, and presents our determination of Φ_{FQY} for CO₂ UV LIF to enable quantitative LIF of hot CO₂.

2.2 CO₂ UV spectroscopy

Although exact mechanisms for CO₂ UV LIF have yet to be clearly identified and are a topic for further research, we present here a brief discussion of the current understanding of CO₂ spectroscopy leading to UV LIF.

2.2.1 CO₂ electronic structure

The electronic ground state of CO₂ is a $1^1\Sigma_g^+$ state with linear (point group $D_{\infty h}$) symmetry [15]. The highest occupied molecular orbital (HOMO) is a degenerate π_g orbital, followed by a σ_u orbital; the lowest unoccupied molecular orbital (LUMO) is a degenerate π_u^* orbital. The lowest-energy molecular orbital (MO) excitation is expected to be $1\pi_g \rightarrow 2\pi_u$, which gives rise to $1,3\Sigma_u^-$, $1,3\Delta_u$, and $1,3\Sigma_u^+$ excited states. The other low-energy MO excitation is $3\sigma_u \rightarrow 2\pi_u$, yielding $1,3\Pi_g$ excited states, depending on the electron spins and the partitioning in the molecular orbital. Calculations have shown that the lowest excited electronic states of CO₂ are $3B_2$, $3A_2$, $1A_2$, $1B_2$, which all have bent symmetry (point group C_{2v}) [16]. For the bent $1,3B_2$ states, the energy versus the OC–O distance is plotted qualitatively in Fig. 2 (taken from [17]). Note that the singlet and triplet potential surfaces cross and inter-system crossing (ISC) via spin change can take place.

2.2.2 State energies from CO₂ absorption data

CO₂ absorption cross-section measurements using shock-heated CO₂ [14] show that the absorption cross-section (σ) increases with temperature at fixed wavelength, and the plot of $(\ln \sigma)$ vs. $(1/T)$ was found to be linear for $900 < T < 2500$ K (note the data range in [14] is $1500 < T < 4500$ K). From the slope of the linear fits, the ground-state energy involved in the excitation was estimated, and interpreted as the amount of excitation of the bending vibrational mode necessary to yield significant Franck–Condon (FC) overlap factors with the bent excited states of CO₂, and such results are presented in Table 1.

The data in Table 1 suggest that UV light absorption in the 200–300 nm range will lead to population of the bent

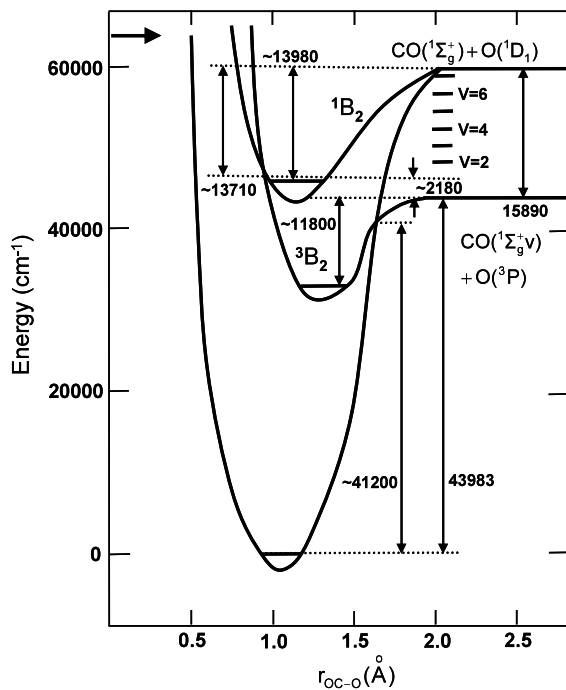


Fig. 2 Potential energy curves for CO₂ [17]. Intersystem crossing occurs between the ^{1,3}B₂ states

Table 1 Analysis of the ground state and excited state energies for various excitation wavelengths including the ones used in this study

Excitation λ [nm]	Photon energy [eV]	Ground-state energy [eV]	Excited-state energy [eV]
215.00	5.77	1.07	6.84
220.00	5.64	1.14	6.78
225.00	5.51	1.21	6.72
230.00	5.39	1.28	6.67
235.00	5.28	1.35	6.63
239.34	5.18	1.41	6.59
242.14	5.12	1.45	6.57
245.00	5.06	1.49	6.55
250.00	4.96	1.56	6.52

¹B₂ state, in which the lowest energy level is 5.74 eV above the ground state energy. As the excitation wavelength increases (excitation energy decreases) the amount of internal energy in the CO₂ ground state must increase to conserve energy and population in the bending vibration is required for efficient excitation of CO₂. The same excited state is also populated by the CO(¹Σ⁺) + O(³P) recombination reaction which produces the so-called CO flame bands, which is described briefly in Sect. 2.3.

2.2.3 CO₂-LIF emission

The overall laser-induced fluorescence signal of CO₂ can be expressed by the following equation:

$$S_{LIF} = I_{Laser} \cdot \frac{A}{h\nu} \cdot l \cdot n_{CO_2} \cdot \sigma_{CO_2} \cdot \Phi_{FQY} \cdot \left(\frac{\Omega}{4\pi}\right) \cdot R_{LIF}, \tag{1}$$

where S_{LIF} is the LIF signal intensity (integrated over the fluorescence wavelength region), I_{Laser} is the laser fluence passing through the probe volume, A is the cross-sectional area illuminated by the laser beam, l is the length of the probe volume, $h\nu$ is the laser energy per photon, n is the number density of the CO₂, σ_{CO_2} is the absorption cross-section, Φ_{FQY} is the fluorescence quantum yield (not to be confused with fuel/air equivalence ratio ϕ), $(\Omega/4\pi)$ is the fraction of the solid angle collected by the lens or detector, and R_{LIF} is the average spectral responsivity of the optics and the detector system. The terms of $I_{Laser} \cdot A/h\nu \cdot l \cdot (\Omega/4\pi) \cdot R_{LIF}$ can be collected as a constant c , giving:

$$S_{LIF,CO_2} = c \cdot n_{CO_2} \cdot \sigma_{CO_2} \cdot \Phi_{FQY}. \tag{2}$$

In Sect. 4.1, we will discuss in further detail of how the CO₂ Φ_{FQY} is determined by comparing the relative LIF signal of CO₂ to that of NO at a specific well-defined condition.

2.3 Fluorescence quantum yield

The available photophysics literature for CO₂ is reviewed [12–25], to help us determine the CO₂ Φ_{FQY} , which is the

Table 2 Analysis of the ground state and excited state energies for various excitation wavelengths including ones used in this study

Number	Reaction	Notation	Description
(1)	$\text{CO}_2(^1\Sigma_g^+) + h\nu \rightarrow \text{CO}_2(^1\text{B}_2)$	<i>Ab</i>	Absorption into $^1\text{B}_2$
(2)	$\text{CO}_2(^1\text{B}_2) \rightarrow \text{CO}_2(^1\Sigma_g^+) + h\nu$	<i>A</i>	Fluorescence from $^1\text{B}_2$
(3)	$\text{CO}_2(^1\text{B}_2) \rightarrow \text{CO}_2(^3\text{B}_2)$	<i>ISC</i>	Spin change
(4)	$\text{CO}_2(^1\text{B}_2) + \text{M} \rightarrow \text{CO}_2(^1\Sigma_g^+)$	<i>Q₁</i>	Quenching of $^1\text{B}_2$
(5)	$\text{CO}_2(^3\text{B}_2) + \text{M} \rightarrow \text{CO}_2(^1\Sigma_g^+)$	<i>Q₃</i>	Quenching of $^3\text{B}_2$
(6)	$\text{CO}_2(^3\text{B}_2) \rightarrow \text{O}(^3\text{P}) + \text{CO}(^1\Sigma^+)$	<i>D</i>	Dissociation out of $^3\text{B}_2$

ratio of the rate of fluorescence and the sum of rates of all the de-excitation pathways of the excited state:

$$\Phi_{\text{FQY}} = \frac{A}{\text{ISC} + A + Q}, \quad (3)$$

where *A* is the fluorescence rate, *ISC* the rate for intersystem crossing between the excited singlet state and an overlapping triplet state, and *Q* the rate of collisional quenching. The most relevant de-excitation pathways are listed in Table 2.

Absorption (Equation (1) in Table 2) As discussed in the previous section, absorption occurs out of vibrationally-excited modes of the ground state into the bent $^1\text{B}_2$ states. State energies of CO_2 indicate that for excitation wavelengths relevant to this study (210–260 nm), CO_2 is excited into levels of the $^1\text{B}_2$ state with a total energy of ca. 6.5–6.9 eV. There also may be some absorption into the $^1\text{A}_2$ state; however, this is expected to be much weaker and of negligible impact in the LIF process [16].

Radiation (Equation (2) in Table 2) Broadband radiation out of the $^1\text{B}_2$ state has been documented for CO_2 as far back as the 1930 [19]. The faint continuous spectra of $\text{CO} + \text{O}_2$ flames (“CO flame bands” at 250–800 nm) have been attributed to this radiative process [22]. Similar emission is also observed from $\text{CO} + \text{O}$ reactions in discharge tubes (after dissociation of CO_2 or by reaction of CO with independently produced O atoms) [25], in shock tubes (after dissociation of CO_2) [25], and also in flames [25]. The fluorescence rate calculated from kinetic data is projected to be approximately $A = 2\text{--}6 \times 10^6 \text{ s}^{-1}$ [26]. The blue-shift of the CO_2 -LIF emission in comparison to the luminescence from the CO flame bands is still unclear. Excitation for CO_2 mainly occurs into levels 5.8–6.2 eV above the ground state while the $\text{CO} + \text{O}$ system at 2600 K (adiabatic flame temperature) has a total internal energy of ~ 6.48 eV above the CO_2 ground state. However, excited CO_2 formed from the $\text{CO} + \text{O}$ reaction may require ISC ($^3\text{B}_2 \rightarrow ^1\text{B}_2$) at a lower energy threshold than the direct UV excitation used in this study. In addition, third-body reactions involved in $\text{CO} + \text{O}$

reactions may also contribute to fluorescence of lower energy. Further study of excited upper levels of CO_2 leading to LIF emission is needed for a complete understanding.

Inter-system crossing (Equation (3) in Table 2) Singlet-triplet crossing is very effective ($\text{ISC} > 10^9 \text{ s}^{-1}$) across the $^1\text{B}_2$ and $^3\text{B}_2$ potential surfaces [26]. The fast spin-changing mechanism is proposed as an explanation for the experimental observation of a linear laser-energy dependence (single-photon absorption; no saturation because of fast ISC), linear pressure dependence (fluorescence lifetime is not quenching limited due to fast ISC) and fast fluorescence decay time (5 ns upper limit). It also should be noted that the surface-crossing point probably is close to the $^1\text{B}_2$ ground state energy (which we estimate to be 5.74 eV above the electronic ground state) [16].

Quenching (Equations (4), (5), and (6) in Table 2) There is no extensive study of CO_2 quenching available in the current literature. Quenching of the $^1\text{B}_2$ state is slower than ISC ($^1\text{B}_2 \rightarrow ^3\text{B}_2$) since the LIF data reported below show that Φ_{FQY} is constant for pressures up to 60 bar. Φ_{FQY} in this case is limited by the fast ISC and not by quenching. Dissociation (6) is only possible after spin crossing (direct dissociation to O (^1D) requires 7.41 eV, while dissociation to O (^3P) only 5.45 eV). Due to the fast ISC, most of the initial population is expected to arrive in the $^3\text{B}_2$ state where the Φ_{FQY} is small. Since photodissociation yields of CO_2 are typically 10–20% in the wavelength range of 226–230 nm [1, 27, 28], Q_3 is expected to be a few times larger (4–9) than the dissociation rate at our experimental conditions.

3 Experimental

3.1 Experimental setup

The apparatus and setup used in this study have been previously described [8–10] and will be discussed only briefly here. Laminar, premixed CH_4/air and $\text{CH}_4/\text{Ar}/\text{O}_2$ flat-flames at pressures from 10–60 bar were stabilized on a porous, sintered stainless matrix of 8 mm diameter. This

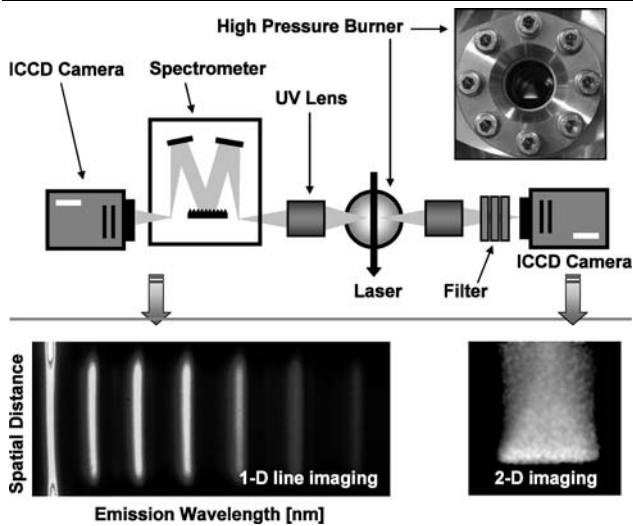


Fig. 3 Experimental setup for 1-D line imaging (*left*) and 2-D imaging (*right*). Resulting images are shown on the *bottom*

burner was mounted in a pressurized vessel with an inner diameter of 60 mm with stabilization to ± 0.1 bar. Investigations were conducted for various CH_4/air equivalence ratios ($\phi = 0.8\text{--}1.5$). Optical access to the flame was possible via four quartz windows (Heraeus, Suprasil 2 grade). Laser pulse energy ranged from 0.8–1.2 mJ/pulse (7 ns pulse at 10 Hz with linewidth of 0.2 cm^{-1}) from a Nd:YAG-pumped (Quanta Ray GCR250) frequency-doubled (BBO) dye laser (LAS, LDL205). For spectrally-resolved 1-D line imaging measurements, the beam was weakly focused (diameter = 1 mm) along a line 3 mm above the burner matrix and crosses the flame horizontally (Fig. 3, left side). The pulse energy was monitored with a photodiode (LaVision). Fluorescence signals were collected at right angles to the laser beam and focused with an $f = 105$ mm, $f\# = 4.5$ achromatic UV-lens (Nikon), dispersed spectrally through an imaging spectrometer (LaVision Chromex 250IS) and imaged onto an intensified CCD camera (LaVision DynaMight). The resulting image is shown in Fig. 3, where the spectral information is shown on the horizontal axis and the spatial information along the laser is shown on the vertical axis. Relative spectral response of the spectrometer was calibrated using a D_2 lamp. For 2-D imaging measurements, the laser was optically stretched into a vertical sheet ($0.5 \times 15\text{ mm}^2$) and imaged directly using an ICCD camera with a filter set for suppression of Rayleigh scattering and bandpass filtering (Fig. 3, right side). The signals from 20 laser pulses were accumulated on the camera chip. Specific choice of excitation wavelength (λ) and detection bandpass will be discussed in Sect. 3.3.

3.2 Temperature

Temperature is a critical parameter in dealing with laser-induced fluorescence as it impacts many relevant terms

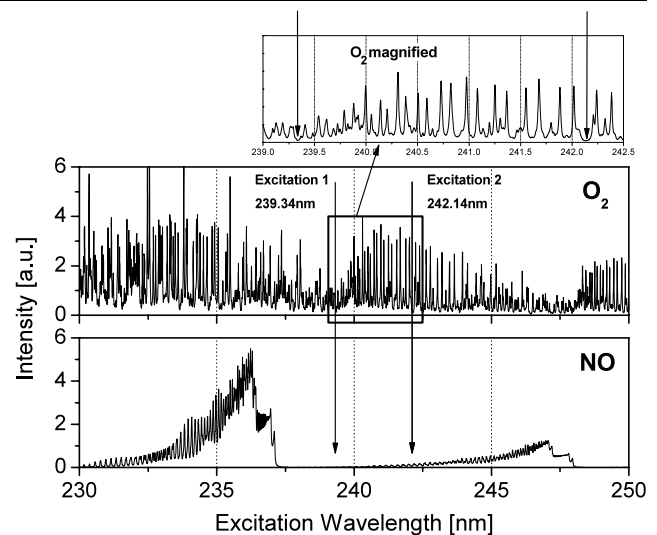


Fig. 4 Simulated LIF excitation spectra of O_2 (*upper frame*) and NO (*lower frame*) at 20 bar and 2000 K (LIFSim [32]). A magnified O_2 LIF spectrum near the excitation wavelengths (239.34 nm and 242.14 nm shown with *arrows*) is shown at the *top*

such as the population of the laser-excited ground state, the spectral overlap between the laser-spectral profile and the absorption spectrum, and the fluorescence quantum yield (Φ_{FQY}). To obtain the temperature dependence of Φ_{FQY} , temperature of the flame was varied by changing the equivalence ratio of the fresh gases ($\phi = 0.8\text{--}1.5$). The absolute value of the temperatures for each equivalence ratio was measured using a previously developed multi-line LIF thermometry technique [29, 30]. We expect that errors in temperature measurements to be within 5% (average error of 1.5%) for all the data presented.

3.3 CO_2 excitation and detection

Excitation of CO_2 in high-pressure flames is complicated by the following issues. Excitation spectra of CO_2 in the 200–300 nm spectral region directly overlap with excitation of the $\text{A}^2\Sigma^+ - \text{X}^2\Pi$ γ bands of NO and the $\text{B}^3\Sigma^- - \text{X}^3\Sigma^+$ Schumann–Runge bands of O_2 [8]. Pressure broadening increases this overlap. Finding an excitation wavelength where interference signals are minimized is difficult due to the pervasive nature of O_2 bands in this region [31]. We have chosen a strategy to use excitation wavelengths which avoids overlap with NO transitions in the region, while at the same time, minimizing the overlap with the multiple vibrational bands of O_2 . The candidate excitation wavelengths were taken from our previous work [2] (239.34 and 242.14 nm), both of which are located between the $\text{A}-\text{X}(0,1)$ and $\text{A}-\text{X}(0,2)$ bands of NO as shown in Fig. 4 (lower plot). These choices minimize contributions of O_2 (Fig. 4, upper plot), as predicted by numerical simulations

(LIFSim [32]), and also confirmed through experimental excitation scans with wavelength-resolved detection in a lean high-pressure flame ($\phi = 0.8$, $p = 10$ bar), where excess O_2 yields identifiable LIF signal in the burned gas. In comparison, excitation at 242.14 nm was found to provide the least interference from O_2 with sufficient NO minimization, while 239.34 nm excitation completely avoids NO excitation at the cost of an increase in O_2 interference.

Possible depletion of the lower state CO_2 population was considered. The CO_2 -LIF signals were linear with excitation laser energy over the full pressure range (10–60 bar). This is consistent with Frank et al. [26] who observed CO_2 -LIF interference in their study of two-photon excited O atoms near 225 nm. They found the CO_2 -LIF began to saturate at a laser fluence of 12 J/cm^2 , which is much larger than the $<0.5 \text{ J/cm}^2$ used for the LIF data reported here. Even though at 20 bar pressure the excitation laser is attenuated by $\sim 16\%$, at the $\sim 2000 \text{ K}$ flame temperature, only a few percent of the CO_2 molecules with 1 eV or more internal energy are required to produce this absorption.

The CO_2 detection window was selected as 300–350 nm, using a combination of high- and low-pass filters (Optosigma and Asahi Optics) and an additional 280 nm high-pass filter (Optosigma) for suppression of elastic scattering of the laser at higher pressures (>20 bar). This ensures suppression of elastic scattering as well as Raman scattering from other combustion products. Any detection region between 280–370 nm could be used as long as interference from Raman scattering or O_2 -LIF is not present. The 350 nm red limit also suppresses background from flame emission, scattered pump-laser light, and/or room light. With this detection scheme, the correction to the signal for contribution from O_2 and NO interference was less than 5% for the worst case of a $\phi = 0.9$, 60 bar flame.

4 Results

4.1 Determination of CO_2 fluorescence quantum yields by calibration with NO-LIF

To determine of the value of Φ_{FQY} for CO_2 , signals for NO and CO_2 -LIF are imaged onto the slit of the spectrometer using the same excitation laser and detected using the same setup as shown in Fig. 3 in a $\phi = 1.1$, $CH_4/Ar/O_2$ flame with 300 ppm added NO. The LIF signal from both species was collected from the laser-illuminated volume of the burned gases (just past the reaction zone of the flame, 3 mm above burner matrix) in the limit of weak excitation. Note that the excitation wavelength was optimized for simultaneous CO_2 and NO excitation (226.03 nm) and not for 2-D CO_2 imaging as discussed in the previous section.

The ratio of NO- and CO_2 -LIF signal intensities can be written as:

$$\frac{S_{LIF,CO_2}}{S_{LIF,NO}} = \frac{c \cdot n_{CO_2} \cdot \sigma_{abs,CO_2} \cdot \Phi_{FQY,CO_2}}{c \cdot n_{NO} \cdot \sigma_{abs,NO} \cdot \Phi_{FQY,NO}} \quad (4)$$

Note that by simultaneously taking the CO_2 - and NO-LIF with the same experimental setup, c is identical in both cases and cancels out. The beam profile was verified to be constant over the wavelength region used in this study. The other terms can be determined from both experimental data and theoretical calculations. The signal intensity (S_{LIF}) of both CO_2 and NO are determined by integrating the respective LIF signals from a spectrally dispersed emission profile (Fig. 1).

For CO_2 (numerator of (4)), the number density (n) is estimated from chemical equilibrium calculations [33] at the given equivalence ratio and pressure. The absorption cross-section for CO_2 (σ_{abs}) is conceptually an overlap between the spectral profile of the laser and the broadband absorption spectra of CO_2 , which was determined as a function of temperature in recent shock-tube measurements [12, 14].

For NO (denominator of (4)), more care must be taken in describing the LIF signal. Unlike CO_2 , which is excited through a broadband absorption process, NO excitation is governed by the overlap between the spectral width of the laser and a few selected transition lines (dictated by the pressure shift and broadening of the excitation spectra). The LIF signal for NO can also be written as

$$S_{LIF,NO} = c \cdot n_{NO} \cdot f_B \cdot B_{12} \cdot \Gamma \cdot \Phi_{NO}, \quad (5)$$

where f_B is the Boltzmann fraction of the population in the laser excited state, B_{12} is the Einstein coefficient for stimulated absorption, Γ is the spectral overlap of the laser bandwidth with the transition linewidth. For the current study the number density n was calibrated in a lean flame ($\phi = 0.9$) using an NO addition method [29]. By using a lean flame, we can avoid dealing with NO reburn reactions which can strongly influence NO concentrations in rich flames. This quantitative measurement of NO is then used to calibrate the NO-LIF detection in a slightly rich ($\phi = 1.1$) flame under the same detection conditions, where we find 253 ppm of NO (note the input gases contain 300 ppm NO). The absorption cross-section of NO, σ_{abs} , requires detailed information regarding the Boltzmann fraction f_B , the overlap function Γ and the absorption strength B_{12} of relevant transitions, which is complicated by the collisional broadening of the excitation spectra. The determination of Φ_{FQY} of NO also requires accurate information regarding spontaneous emission A_{21} and quenching Q , since $\Phi_{FQY} = A/(A + Q)$. These data were taken from LIFSim [32] based on [34–38]. The value 2.36×10^{-6} was determined for $T = 2000 \text{ K}$, $p = 20 \text{ bar}$, $\lambda_{ex} = 226.03 \text{ nm}$ and $\phi = 1.1$.

4.2 Dependence of the CO₂ fluorescence quantum yield on temperature, pressure and excitation wavelength

Φ_{FQY} was determined as a function of excitation wavelength and flame temperature at 20 bar. The variation of Φ_{FQY} with excitation wavelength was determined by changing the excitation wavelength of the laser (from 215 to 250 nm) and monitoring the relative change in the CO₂-LIF intensity of the entire CO₂-LIF emission (between 200 and 400 nm), and by correcting for absorption effects on both the probe beam and fluorescence caused by hot CO₂ and H₂O (note that CO₂ accounts for >97% of the attenuation). Measurements were carried out in a CH₄/Ar/O₂ flame to eliminate the interference from NO, and in a slightly rich flame to avoid interference from the Schumann–Runge bands of O₂ ($\phi = 1.1$). Based on the data in Fig. 5, the relationship between the excitation wavelength and LIF intensity can be fit to a smooth curve. The ordinate scale of this data curve is calibrated at 226.03 nm (shown in Fig. 5) where a CH₄/air flame was used with 300 ppm of seeded NO to determine

Φ_{FQY} of CO₂ as described above. The values of Φ_{FQY} for a variety of wavelengths extending from 215 to 250 nm at 20 bar are shown in Fig. 5. As shown in Fig. 5, we estimate errors for the Φ_{FQY} to be less than $\pm 0.5 \times 10^{-6}$ over the given conditions based on accumulated uncertainties in all the experimental and computational values (e.g., number density determination, fitting routine for spectral separation, numerical simulation of NO, Φ_{FQY} , etc.). The absolute intensities of the CO₂-LIF as well as the corresponding absorption coefficients are also plotted. It is interesting to note that while the absorption coefficient increases as the excitation wavelength decreases, Φ_{FQY} decreases as the excitation wavelength decreases. The CO₂-LIF signal intensity does not increase as rapidly as the absorption cross-section as the excitation wavelength is decreased towards the UV.

The fluorescence quantum yield of CO₂ as a function of temperature from 1760 to 2025 K at 20 bar is shown in Fig. 6. Table 3 gives a complete listing of our results. Note that 239.34 and 242.14 nm are the excitation wavelengths

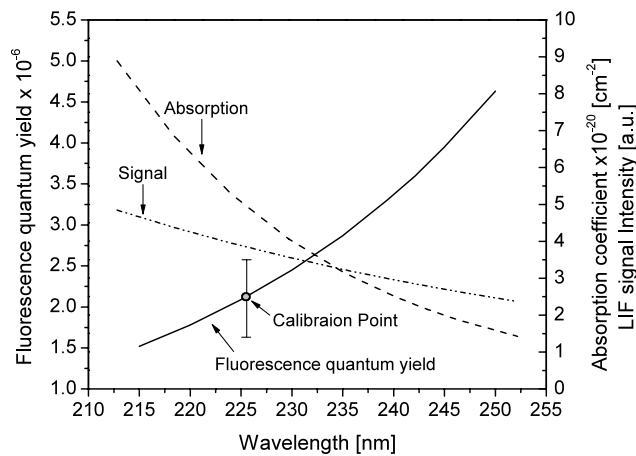


Fig. 5 Fluorescence quantum yield of CO₂ as a function of excitation wavelength at $p = 20$ bar and $T \sim 2000$ K. Signal intensity and absorption coefficient are also plotted

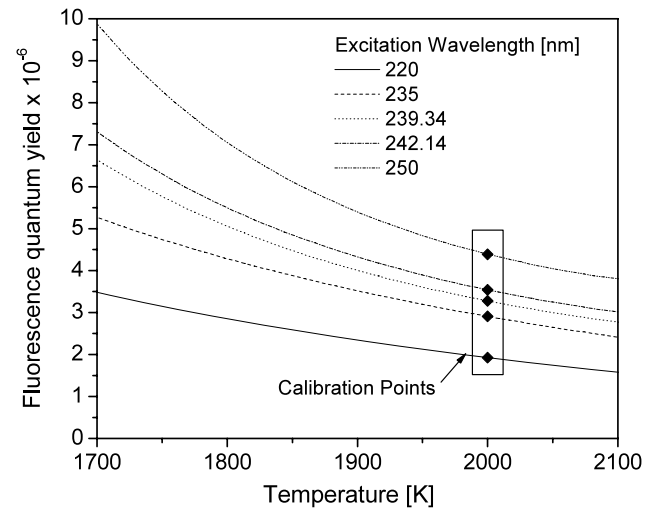


Fig. 6 Fluorescence quantum yield of CO₂ as a function of excitation wavelength and temperature at 20 bar

Table 3 Measured fluorescence quantum yields Φ_{FQY} of CO₂ for $215 \leq \lambda \leq 250$ nm, and $1760 \leq T \leq 2025$ K

	2025 K	2000 K	1960 K	1925 K	1890 K	1860 K	1830 K	1760 K
215 nm	1.61E-06	1.68E-06	1.80E-06	1.97E-06	2.12E-06	2.30E-06	2.50E-06	3.07E-06
220 nm	1.83E-06	1.93E-06	2.06E-06	2.24E-06	2.38E-06	2.54E-06	2.70E-06	3.09E-06
225 nm	2.12E-06	2.21E-06	2.35E-06	2.54E-06	2.70E-06	2.86E-06	3.03E-06	3.46E-06
230 nm	2.42E-06	2.54E-06	2.70E-06	2.92E-06	3.10E-06	3.28E-06	3.47E-06	3.93E-06
235 nm	2.78E-06	2.91E-06	3.10E-06	3.36E-06	3.58E-06	3.81E-06	4.05E-06	4.65E-06
239.34 nm	3.13E-06	3.28E-06	3.50E-06	3.80E-06	4.08E-06	4.38E-06	4.72E-06	5.62E-06
242.14 nm	3.39E-06	3.54E-06	3.77E-06	4.11E-06	4.41E-06	4.74E-06	5.11E-06	6.13E-06
245 nm	3.67E-06	3.83E-06	4.08E-06	4.44E-06	4.77E-06	5.14E-06	5.55E-06	6.70E-06
250 nm	4.21E-06	4.39E-06	4.68E-06	5.11E-06	5.51E-06	5.97E-06	6.50E-06	8.01E-06

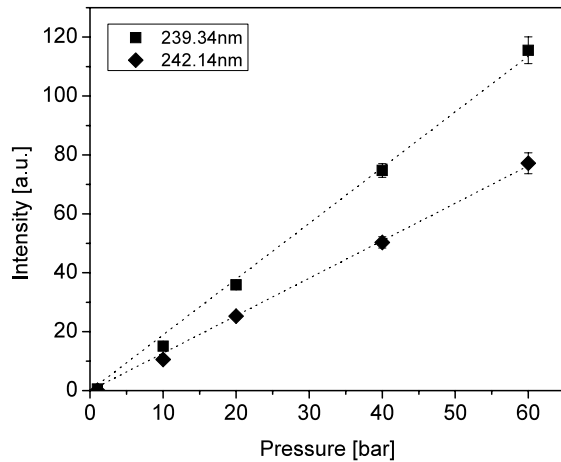


Fig. 7 Dependence of CO₂-LIF intensity on pressure for excitation wavelengths of 239.34 and 242.14 nm at 20 bar (CH₄/air flame with $T \sim 2000$ K and $\phi = 0.9$)

chosen for the LIF measurements in this study. The temperature of the flame was varied by changing the equivalence ratio of the fresh gases ($\phi = 0.8$ – 1.5). The variation in LIF signal for each excitation wavelength (Table 3) was calibrated at 2000 K. These data were fit using a second-order polynomial to generate the trends shown in Fig. 6. The calibration points are also shown in Fig. 6. The absolute values of Φ_{FQY} at the calibration temperature of ~ 2000 K have been taken from Fig. 5. Although the absorption cross-section decreases at low temperatures, this is somewhat offset by the increase of the Φ_{FQY} , allowing for potential use of CO₂-LIF at lower temperatures.

The fluorescence quantum yield of CO₂ has no measurable dependence on pressure. The quenching rate Q increases with pressure. The CO₂ mole fraction is essentially independent on pressure for these flames and thus the number density of CO₂ increases with pressure. Thus, if collisional quenching was the dominant loss mechanism for excited CO₂ molecules, the LIF signal would be independent of pressure. However, as shown in Fig. 7, the LIF signal increases linearly with pressure and thus increases with the CO₂ number density. This indicates that Φ_{FQY} for CO₂ is constant for the pressure range studied. We postulate that intersystem crossing (ISC: $^1\text{B}_2 \rightarrow ^3\text{B}_2$), dominates the loss of excited CO₂. Due to the constant Φ_{FQY} with pressure, UV LIF of CO₂ is particularly suited for detection of CO₂ in applications at elevated pressures; whereas more typically, LIF signals decrease with pressure because collisional quenching is usually the dominant loss mechanism.

4.3 Demonstration of quantitative LIF imaging of CO₂

Quantitative UV LIF of CO₂ requires temperature information. Temperature influences the overall LIF signal via the temperature dependence of the absorption cross-section and

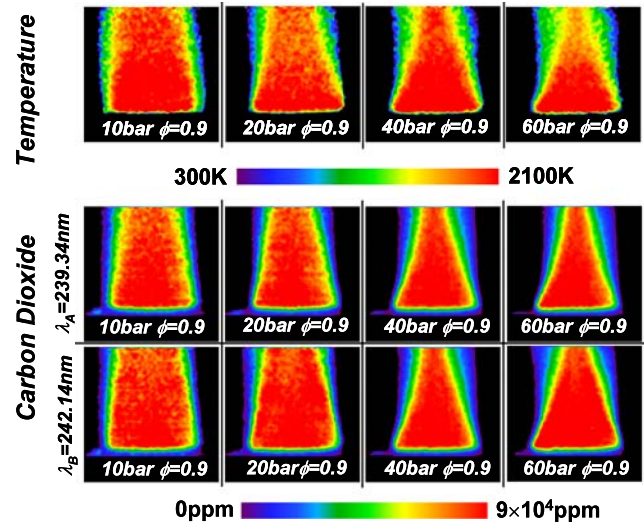


Fig. 8 Temperature fields obtained from two-line NO-LIF thermometry (*above*) and PLIF images of CO₂ mole fractions from a $\phi = 0.9$ CH₄ flames for pressures of 10–60 bar. Results with two different excitation wavelengths (239.34 and 242.14 nm) are shown

the modest temperature variation of Φ_{FQY} . Temperature is also required to correct for laser and fluorescence signal attenuation. Two-line NO-LIF thermometry offers a non-intrusive method to measure 2-D temperature images with relatively high precision. With the current setup, temperatures are within $\pm 5\%$ at 2000 K (at 20 bar) using a single point thermocouple calibration. The temperature fields obtained via 2-D 2-line thermometry using NO-LIF (line selection, 226.03 and 225.487 nm using 300 ppm NO seeding) are shown in the upper portion of Fig. 8. A detection window centered at 254 nm (FWHM 17.5 nm; Asahi Optics) was used to maximize the purity of the NO-LIF signal. These NO-LIF temperatures fields are used to process the CO₂-PLIF images in the lower portion of Fig. 8.

The LIF images of hot CO₂ in the high-pressure burned gases are shown in the lower portion of Fig. 8 for 10–60 bar using two excitation wavelengths (239.34 and 242.12 nm). The images have been averaged over 40 laser shots and the resulting signal-to-noise ratio (SNR) ranges from ~ 55 (60 bar) to ~ 120 (10 bar). The LIF signal is calibrated at a single point 3 mm above the burner matrix in the 20 bar flame. The CO₂ concentration is taken from a 1-D simulation of the burned gas (Chemkin Premix from Reaction Design), and this value provides the needed calibration of the collection efficiency and detection solid angle. The visualization of CO₂ is more accurate near the center of the burned gas cone and becomes less reliable around the edges as stability of flame decreases and temperature gradients are steep. The intensity of the laser pulse and the resulting fluorescence were corrected for absorption mainly from hot CO₂. As previously mentioned, the interference from O₂ and NO (O₂ is the dominant source of interference)

combined is expected to be less than 4% for these flames which have an equivalence ratio of 0.9. The uncertainty is smaller for fuel rich (ϕ below onset of LIF of polycyclic aromatic hydrocarbons) flames as O_2 concentration is further reduced. It should be noted that the averaging used here is not suitable for turbulent flows where higher laser pulse energy will be needed for single shot imaging with adequate SNR.

5 Conclusions

We present the quantitative determination of the fluorescence quantum yield (Φ_{FQY}) of CO_2 -LIF as a function of wavelength (215–250 nm) and temperature (1760–2025 K) using 1-D line imaging of hot carbon dioxide LIF in a laminar high-pressure flame (CH_4 /air) over a pressure range of 10 to 60 bar. Φ_{FQY} of CO_2 is determined by comparing the relative intensity of CO_2 -LIF to that of nitric oxide LIF while simultaneously exciting both species and by using CO_2 concentrations from 1-D flame simulations. Φ_{FQY} of CO_2 increases with wavelength in our detection range and decreases with temperature. The accuracy of the temperature dependence of CO_2 fluorescence quantum yield could be further enhanced if data were available over a larger range of temperature. Φ_{FQY} of CO_2 is found to be independent of pressure which indicates that collisional quenching is significantly slower than other losses of the excited CO_2 . This effect is believed to be a consequence of fast inter-system crossing which dominates the population depletion dynamics of laser-excited CO_2 .

Two wavelengths (239.34 and 242.14 nm) optimized to minimize interference from O_2 and NO-LIF signals were used to demonstrate quantitative LIF imaging of CO_2 over a pressure range of 10 to 60 bar. The ability to image CO_2 concentration in combustion environments can potentially offer a powerful tool for the study of fundamental combustion and/or optimization of more efficient combustors.

Acknowledgements This work is supported by the Air Force Office of Scientific Research (AFOSR) with Dr. Julian Tishkoff as program manager. CS and WB thank the German Research Foundation (DFG) for support.

References

1. W.G. Bessler, C. Schulz, T. Lee, J.B. Jeffries, R.K. Hanson, *Chem. Phys. Lett.* **375**, 344–349 (2003)
2. T. Lee, W.G. Bessler, C. Schulz, M. Patel, J.B. Jeffries, R.K. Hanson, *Appl. Phys. B* **79**, 427–430 (2004)
3. A.C. Eckbreth, *Laser Diagnostics for Combustion Temperature and Species* (Gordon & Breach, Amsterdam, 1996)
4. J. Wolfrum, *Proc. Combust. Inst.* **27**, 1–41 (1998)
5. K. Kohse-Höinghaus, J.B. Jeffries, *Applied Combustion Diagnostics* (Taylor & Francis, London, 2002)
6. B.J. Kirby, R.K. Hanson, *Appl. Opt.* **41**, 1190–1201 (2002)
7. B.J. Kirby, R.K. Hanson, *Appl. Opt.* **40**, 6130–6144 (2001)
8. W.G. Bessler, C. Schulz, T. Lee, J.B. Jeffries, R.K. Hanson, *Appl. Opt.* **42**, 4922–4936 (2003)
9. W.G. Bessler, C. Schulz, T. Lee, J.B. Jeffries, R.K. Hanson, *Appl. Opt.* **42**, 2031–2042 (2003)
10. W.G. Bessler, C. Schulz, T. Lee, J.B. Jeffries, R.K. Hanson, *Appl. Opt.* **41**, 3547–3557 (2002)
11. F. Hildenbrand, C. Schulz, *Appl. Phys. B* **73**, 165–172 (2001)
12. C. Schulz, J.D. Koch, D.F. Davidson, J.B. Jeffries, R.K. Hanson, *Chem. Phys. Lett.* **355**, 82–88 (2002)
13. C. Schulz, J.B. Jeffries, D.F. Davidson, J.D. Koch, J. Wolfrum, R.K. Hanson, *Proc. Combust. Inst.* **29**, 2725–2742 (2002)
14. M.A. Oehlschlaeger, D.F. Davidson, J.B. Jeffries, R.K. Hanson, *Chem. Phys. Lett.* **399**, 490–495 (2004)
15. J.W. Rabalais, J.M. McDonald, V. Scherr, S.P. McGlynn, *Chem. Rev.* **71**, 73–108 (1971)
16. A. Spielfiedel, N. Feautrier, C. Cossart-Magos, G. Chambaud, P. Rosmus, H.-J. Werner, P. Botschwina, *J. Chem. Phys.* **97**, 8382–8388 (1992)
17. D. Harding, R.E. Weston Jr., G.W. Flynn, *J. Chem. Phys.* **88**, 3590–3598 (1988)
18. Y. Matsumi, N. Shafer, K. Tonokura, M. Kawasaki, Y. Huang, R.J. Gordon, *J. Chem. Phys.* **95**, 7311–7316 (1991)
19. M. Koshi, M. Yoshimura, H. Matsui, *Chem. Phys. Lett.* **176**, 519–525 (1991)
20. A.P. Nefedov, V.A. Sinel'shchikov, A.D. Usachev, A.V. Zobnin, *Appl. Opt.* **37**, 7729–7736 (1998)
21. V. Kondratjew, *Z. Phys.* **63**, 322–333 (1930)
22. R.N. Dixon, *Proc. R. Soc. Lond. Ser. A* **275**, 431–446 (1963)
23. R.N. Dixon, *Discuss. Faraday Soc.* **35**, 105–112 (1963)
24. M. Slack, A. Grillo, *Combust. Flame* **59**, 189–196 (1985)
25. C.J. Malerich, J.H. Scanlon, *Chem. Phys. Lett.* **110**, 303–313 (1986)
26. M.C. Lin, S.H. Bouer, *J. Chem. Phys.* **50**, 3377–3391 (1969)
27. J.H. Frank, X. Chen, B.D. Patterson, T.B. Settersten, *Appl. Opt.* **43**, 2588–2597 (2004)
28. T.B. Settersten, A. Dreizler, B.D. Patterson, P.E. Schrader, R.L. Farrow, *Appl. Phys. B: Lasers Opt.* **76**, 479–482 (2003)
29. T. Lee, W.G. Bessler, H. Kronemayer, C. Schulz, J.B. Jeffries, *Appl. Opt.* **44**, 6718–6728 (2005)
30. W.G. Bessler, C. Schulz, *Appl. Phys. B* **78**, 519–533 (2004)
31. G. Herzberg, *Spectra of Diatomic Molecules* (Krieger, Malabar, 1950)
32. W.G. Bessler, C. Schulz, V. Sick, J.W. Daily, A versatile modeling tool for nitric oxide LIF spectra, in *3rd Joint Meeting US Sec. Combust. Inst., Chicago* (2003). www.lifsim.com
33. W. Reynolds, *Stanjan: Chemical Equilibrium Solver* (Stanford University, Stanford, 1987)
34. L.G. Piper, L.M. Cowles, *J. Chem. Phys.* **85**, 2419–2422 (1986)
35. P.H. Paul, *J. Quant. Spectrosc. Radiat. Transf.* **57**, 581–589 (1997)
36. P.H. Paul, J.A. Gray, J.L. Durant Jr., J.W. Thoman, *Chem. Phys. Lett.* **259**, 508–541 (1996)
37. P.H. Paul, J.A. Gray, J.L. Durant Jr., J.W. Thoman, *AIAA J.* **32**, 1670–1675 (1994)
38. J.R. Reisel, C.D. Carter, N.M. Laurendeau, *J. Quant. Spectrosc. Radiat. Transf.* **47**, 43–54 (1982)